

# Fracture toughness of polypropylene copolymers: influence of interparticle distance and temperature

J. U. Starke<sup>a</sup>, G. H. Michler<sup>a</sup>, W. Grellmann<sup>a,\*</sup>, S. Seidler<sup>b</sup>, M. Gahleitner<sup>c</sup>, J. Fiebig<sup>c</sup> and E. Nezbedova<sup>d</sup>

<sup>a</sup>Martin-Luther-University Halle-Wittenberg, Institute of Materials Science, 06217 Merseburg, Germany

<sup>b</sup>Technical University Wien, Institute of Materials Science and Testing, 1040 Wien, Austria

<sup>c</sup>PCD Polymere GmbH, 4021 Linz, Austria

<sup>d</sup>Polymer Institute, 65649 Brno, CZ

(Received 27 November 1996)

A heterophasic reactor grade polypropylene-ethylene copolymer (RAHECO®) was diluted with a propylene-ethylene random copolymer to get materials with constant EPR/PE-particle diameter but various interparticle distances. According to the results of instrumented impact tests, brittle-to-tough transitions were found at  $-20^{\circ}\text{C}$ ,  $-10^{\circ}\text{C}$ ,  $0^{\circ}\text{C}$ ,  $+10^{\circ}\text{C}$  and room temperature. The critical interparticle distance shifts linearly over the range of temperatures from about  $0.4\ \mu\text{m}$  at  $-20^{\circ}\text{C}$  to  $1.3\ \mu\text{m}$  at room temperature. The results were compared with measurements of conventional notched Charpy impact strength at room temperature. The transition from brittle to tough impact behaviour was correlated to a transition of micromechanical deformation mechanisms from cavitation bands to croids. Cavitation of the rubber particles was always the first step of deformation. The in situ HVEM investigations additionally show that the particle distribution should be as homogeneous as possible.  
 © 1997 Elsevier Science Ltd.

(Keywords: polypropylene copolymers; brittle tough transition)

## INTRODUCTION

Polypropylene (PP) is characterised by a poor low temperature impact behaviour because of its relatively high glass transition temperature  $T_g$ . The incorporation of elastomer particles offers a classical solution of this problem. Heterophasic PP blends with increased toughness were first developed by melt compounding PP with different polyolefines (HDPE)<sup>1</sup> or prefabricated ethylene-propylene copolymers (EPR)<sup>1,2</sup> as well as ethylenediene terpolymers (EPDM)<sup>3</sup>. Particularly, PP/EPR blends have been more effectively produced by polymerisation of the monomers directly in the reactor<sup>4</sup>. In this way, it is possible to get materials with distinctive, well dispersed morphologies. Besides the amorphous EPR phase, the modifier particles in these so called 'reactor blends' can also contain crystalline polyethylene (PE). The PE lamellas are generally enveloped in the EPR phase which is useful as compatibilising agent between the semi-crystalline PP matrix and PE.

The size, shape and spatial packing of elastomer particles varied by manufacturing and processing conditions are important parameters in controlling the micromechanical<sup>5</sup> and mechanical<sup>6,7</sup> behaviour of PP/EPR blends. Wu<sup>8</sup> explained that a critical interparticle distance or critical matrix ligament thickness  $A_{\text{crit}}$  exists below which the notched Izod impact strength of nylon blends rapidly

increases. He defined this increase of notched Izod impact strength as brittle-to-tough transition and the critical value of  $A_{\text{crit}}$  as a specific parameter of the material. However, Borggreve *et al.*<sup>9,10</sup> and later Margolina<sup>11</sup> showed that the critical interparticle distance in nylon blends is strongly affected by rate, method of loading and test temperature. They found for instance that  $A_{\text{crit}}$  indeed decreases approximately linearly with temperature.

The nature of transition from brittle to ductile mode of failure is controversially discussed. Besides Wu's percolation theory<sup>8</sup>, another interpretation<sup>7,9,12,13</sup> exists which assumes that stress field overlap begins if the interparticle distance is lower than  $A_{\text{crit}}$ .

Changes from plane strain to plane stress conditions in thinner matrix ligaments, reducing the critical stress for matrix yielding, are preferred by Margolina *et al.*<sup>14,15</sup>. Although the concept is generally accepted, the reduction of the critical stress for matrix yielding cannot explain the frequently investigated changes of micromechanical deformation processes in the interval of brittle-to-tough transition<sup>16,17</sup>. For toughened PP blends, both crazing and shear yielding have been described with respectively brittle and tough fracture<sup>3,18</sup>. However, van der Wal and Gaymans<sup>19</sup> did not find any evidence of crazing in PP/EPDM. They showed that crack tip blunting, melt blunting mechanisms at high testing speeds and cavitation of the rubber particles were the main mechanisms of plastic deformation. Particularly, effects of particle cavitation in toughened plastics have been analysed in detail by Lazzeri and Bucknall<sup>20</sup>.

\* To whom correspondence should be addressed

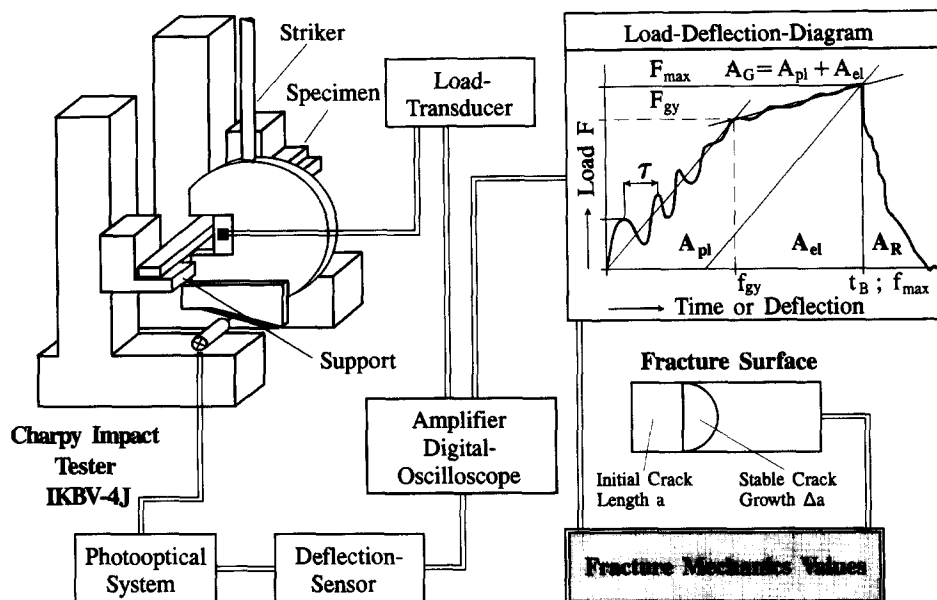


Figure 1 Experimental equipment of instrumented impact tests.

Many explanations have been proposed for brittle-to-tough transition in several nylon/rubber materials and PP/EPDM blends. That is not the case for PP/EPR copolymers whose industrial employment will expand even more in future. Regarding the low temperature toughness, the aim of the present study is to analyse the impact behaviour of PP/EPR copolymers over a wide range of temperatures and compositions.

## EXPERIMENTAL

By means of an instrumented Charpy impact tester with 4J work capacity, impact measurements were performed at  $-20^{\circ}\text{C}$ ,  $-10^{\circ}\text{C}$ ,  $0^{\circ}\text{C}$ ,  $+10^{\circ}\text{C}$  and  $+23^{\circ}\text{C}$  to determine fracture mechanics values as resistance against instable crack growth (Figure 1). The impact speed was always  $1.5\text{ ms}^{-1}$ .

The PP/EPR copolymers<sup>21</sup> were kindly supplied by PCD Polymere GmbH. The basic material RAHECO<sup>®</sup> (heterophasic random copolymer) was melt compounded with a PP material to lower particle concentrations in a single-screw extruder (Table 1). The PP material used for dilution was an ethylene-propylene random copolymer with comparable characteristics as the PP-matrix material of RAHECO<sup>®</sup>.

The dimensions of the injection moulded specimens were: length,  $L = 80\text{ mm}$ ; width,  $W = 10\text{ mm}$  and thickness,  $B = 4\text{ mm}$ . The samples were notched with a razor blade (notch tip radius =  $0.2\ \mu\text{m}$ ). The test conditions were optimised by simulating specimen loading using a finite element method (FEM)<sup>22</sup>. Based on these FEM results, the experimental parameters initial crack length  $a = 2\text{ mm}$  and support span  $s = 40\text{ mm}$  were selected. The consideration of  $a/W = 0.2$  and  $s/W = 4$  enables the determination of geometry-independent fracture mechanics values<sup>23</sup>. Furthermore, a comparison of experimentally measured and numerically computed J-integral values<sup>22</sup> shows a distinct conformity with results of approximation methods of Merkle and Corten<sup>24</sup> and Sumpter and Turner<sup>25</sup>. J-integral values according to Sumpter and Turner can be calculated as:

$$J_{Qd}^{ST} = \eta_{el} \frac{A_{el}}{B(W-a)} + \eta_{pl} \frac{A_{pl}}{B(W-a)} \frac{W-a_{eff}}{W-a} \quad (1)$$

Table 1 Designation and composition of investigated PP/EPR copolymers

Material	Composition	
	$\varphi_{\text{RAHECO}}/\varphi_{\text{Matrix}}$	(wt. %)
1	100/0	RAHECO
2	90/10	
3	80/20	
4	65/35	
5	50/50	
6	35/65	
7	20/80	
8	10/90	
9	0/100	Matrix material

with

$$\eta_{el} = \frac{2F_{GY} s^2 (W-a)}{f_{GY} E_d B W^3} \Gamma^2(a/W) (1-\nu^2) \quad (2)$$

and

$$\eta_{pl} = 2 - \frac{(1-a/W)(0.892 - 4.476a/W)}{1.125 + 0.892a/W - 2.238(a/W)^2} \quad (3)$$

To ensure statistical safety of J-values as resistance against instable crack growth, ten single edge notched specimens per temperature and material were tested at least. In equation (1),  $A_{el}$  and  $A_{pl}$  represent the elastic and the plastic part of total deformation energy  $A_g$  (Figure 1). The effective crack length  $a_{eff}$  results from:  $a_{eff} = a + \Delta a$ . Stable crack growth  $\Delta a$  is quantified on the fracture surface by light microscopy. The Young's modulus  $E_d$  and the yield stress  $\sigma_y$  were measured at corresponding temperatures averaging values of five unnotched specimens. The Poisson's ratio  $\nu$  of the whole sample is approximately given by 0.38. The force  $F_{gy}$  and the deflection  $f_{gy}$  are defined by means of load-deflection diagrams at the transition point from pure elastic to elastic-plastic material behaviour (Figure 1).  $\Gamma(a/W)$  depicts a fitting function correcting the finite specimen geometry.

The materials used for this investigation additionally were characterised by:

- dynamic mechanical analysis (DMA), to decide  $T_g$  of amorphous PP and EPR rubber;

- differential scanning calorimetry (DSC), to detect the grade of crystallisation;
- further mechanical tests, to determine Charpy impact toughness and flexural modulus  $E_f$  of the materials according to ISO 179/1eU and 178, respectively.
- transmission electron microscopy (TEM), to analyse the morphology of the blends (interparticle distance  $A$ , particle diameter  $D$ ). The investigated sections of about  $0.1 \mu\text{m}$  were microtomed from the bulk at  $-100^\circ\text{C}$  and stained with rutheniumtetroxid ( $\text{RuO}_4$ ) vapour for 18 h.
- high-voltage electron microscopy (HVEM), to observe the micromechanical deformation structures at room temperature by in situ tensile tests of semi-thin sections (thickness:  $0.75 \mu\text{m}$ ).

The summary of performed tests shows the complexity of questions which have to be solved to recognise structure–toughness relationships.

## RESULTS AND DISCUSSION

### Basic characterisation

Figure 2 shows DMA curves of the materials 100/0, 65/35, 35/65 and 10/90. Separately detected  $\tan \delta$  peaks of PP and EPR glass transitions indicate that phase separation takes place during copolymerisation. The maximum of PP in the  $\tan \delta$  versus temperature curves does not shift with decreasing EPR concentration. The PP glass transition temperature of  $-5^\circ\text{C}$  is consequently not affected by

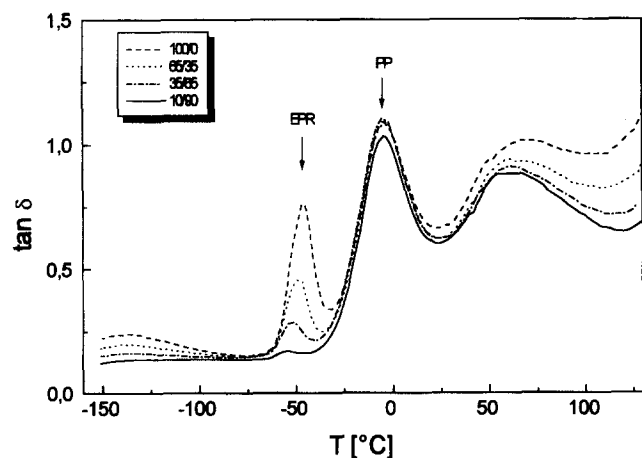


Figure 2 Loss factor  $\tan \delta$  as a function of temperature  $T$  for materials 100/0, 65/35, 35/65 and 10/90. The arrows indicate the position of glass transition temperature of the EPR and amorphous PP phase.

Table 2 Summary of characteristic material parameters

Material	Composition $\phi_{\text{RAHECO}}/\phi_{\text{Matrix}}$ (wt. %)	Glass transition temperature of EPR	Crystallization temperature
		$T_g$ ( $^\circ\text{C}$ )	$T_k$ ( $^\circ\text{C}$ )
1	100/0	-47,1	98,8
2	90/10	-46,8	98,8
3	80/20	-47,6	98,5
4	65/35	-49,9	97,3
5	50/50	-51,3	97,7
6	35/65	-51,8	97,2
7	20/80	-54,4	96,5
8	10/90	-55,0	96,2
9	0/100	—	94,3

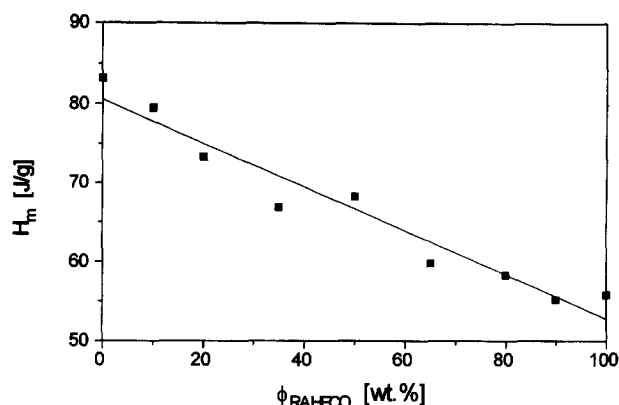


Figure 3 Melt enthalpy  $H_m$  based on DSC measurements of all materials versus RAHECO weight fraction.

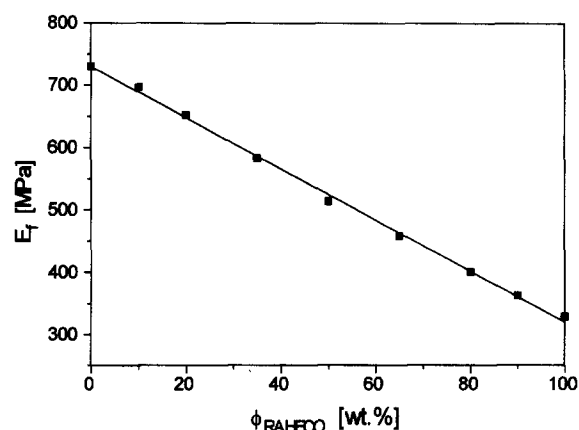


Figure 4 Flexural modulus  $E_f$  versus RAHECO concentration. The continuous slope of  $E_f$  guarantees a linear dilution range to a great extent.

blending processes. In contrast to that, a  $T_g$  shift of EPR was observed. The designated  $T_g$  values of EPR are given in Table 2.

Figure 3 shows the result of DSC measurements, where the melt enthalpy  $H_m$  decreases gradually with increasing EPR content. At the same time, the crystallization temperature  $T_k$  increases due to the nucleation effect of rubber particles (Table 2). In the range of dilution, the expected DSC peak caused by the PE content is only to be detected as a weak shoulder which cannot be evaluated. This implies that the crystalline PE phase is not well developed.

Besides the linear decrease of  $H_m$ , the continuous decrease of flexural modulus  $E_f$  presented in Figure 4 implies that the processing parameters were effectively selected. The result is a system of materials which corresponds to the prescribed mixture relations.

### Morphology

Adjustment of matrix and elastomer viscosity in combination with random copolymerisation of PP with ethylene, which decrease the surface tension between the two phases, realises a very fine morphology of the materials, as illustrated in Figure 5. In the micrographs, the particles appear dark owing to staining with  $\text{RuO}_4$ . Figure 5(b) in particular reveals the internal structure of the particles. They consist of up to five PE-rich inclusions, which are not clearly separated from each other. Within the inclusions, single PE lamellae exist. They are thicker than the PP lamellae of the matrix, so that both kinds of lamellae are

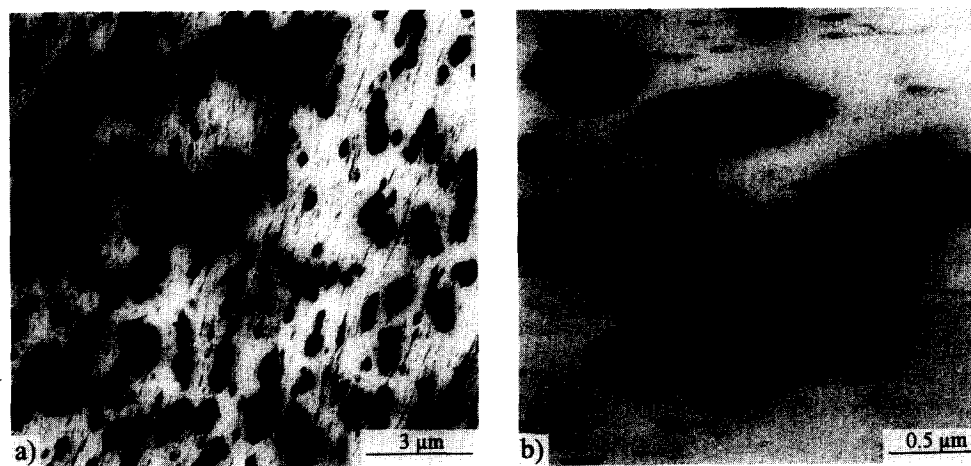


Figure 5 TEM micrographs of material 65/35: (a) Low magnification shows the modifier particle distribution. (b) High magnification represents the internal structure of EPR/PE-particles.

Table 3 Morphological parameters of investigated materials

Material	Composition $\phi_{\text{RAHECO}}/\phi_{\text{Matrix}}$ (wt.%)	Average particle diameter	Average interparticle distance
		D ( $\mu\text{m}$ )	A ( $\mu\text{m}$ )
1	100/0	0,47	0,36
2	90/10	0,50	0,39
3	80/20	0,48	0,40
4	65/35	0,45	0,54
5	50/50	0,46	0,57
6	35/65	0,49	1,00
7	20/80	0,46	1,50
8	10/90	0,47	2,20
9	0/100	—	—

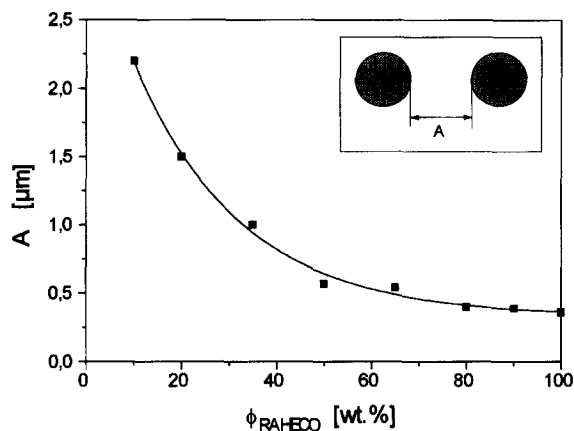


Figure 6 Number-average interparticle distance A versus RAHECO content.

distinguishable. The PE-rich inclusions are surrounded by a dark shining amorphous shell of EPR, providing good adhesion between matrix and modifier particles. Frequently, it is observed that the heterophasic particles are elliptically deformed in the injection moulding direction. The long drawn out ends of the particles are most probably caused by a portion of low molecular weight EPR.

Furthermore, it can be said that the elastomer particles are well dispersed with diameters between 0.1  $\mu\text{m}$  and 2  $\mu\text{m}$ . The number-average particle diameters and interparticle distances of all materials, summarised in Table 3, were obtained from TEM micrographs by image analysis systems

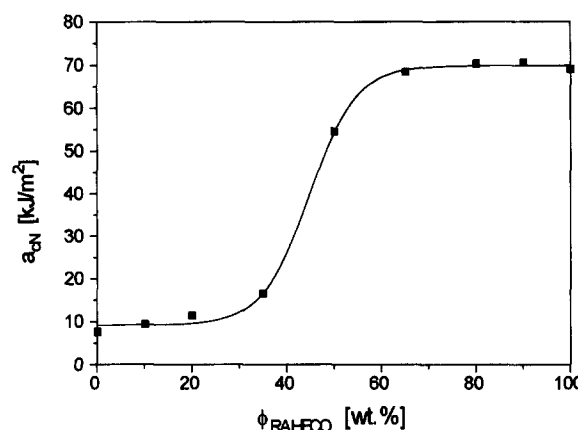


Figure 7 Charpy impact strength at room temperature versus RAHECO content. Particle size and interfacial adhesion are constant.

averaging more than 1000 particles. The average particle diameter D is independent of EPR content and processing conditions and amounts to about 0.47  $\mu\text{m}$ . Figure 6 illustrates the average particle distance A as a function of RAHECO content. It can be observed that the interparticle distance rapidly decreases in the range of RAHECO concentrations from 10 to 50 wt.%, whereas A only gradually decreases between 50 and 100 wt.% of RAHECO.

Mechanical testing

The notched Charpy impact strength ( $a_{\text{CN}}$ ) of all materials measured at room temperature is given in Figure 7. With increasing RAHECO content,  $a_{\text{CN}}$  is approximately constant to 30 wt.%. The transition from moderately to very tough material behaviour is connected with a transition from total to partial fracture. Thereby, the notched Charpy impact strength increases rapidly from about 10  $\text{kJ m}^{-2}$  to 70  $\text{kJ m}^{-2}$ . The transition occurs at about 45 wt.% RAHECO. The flexural modulus decreases continuously with RAHECO content (Figure 4), and the increase of impact strength is not directly affected by the amount of EPR-rubber.

For many industrial applications, the temperature dependence of impact strength is a very interesting point of view. Over the past few years instrumented impact tests<sup>22,23,26</sup> have received increasing attention. Due to the separate registration of the energy components (cf. equation (1)) and

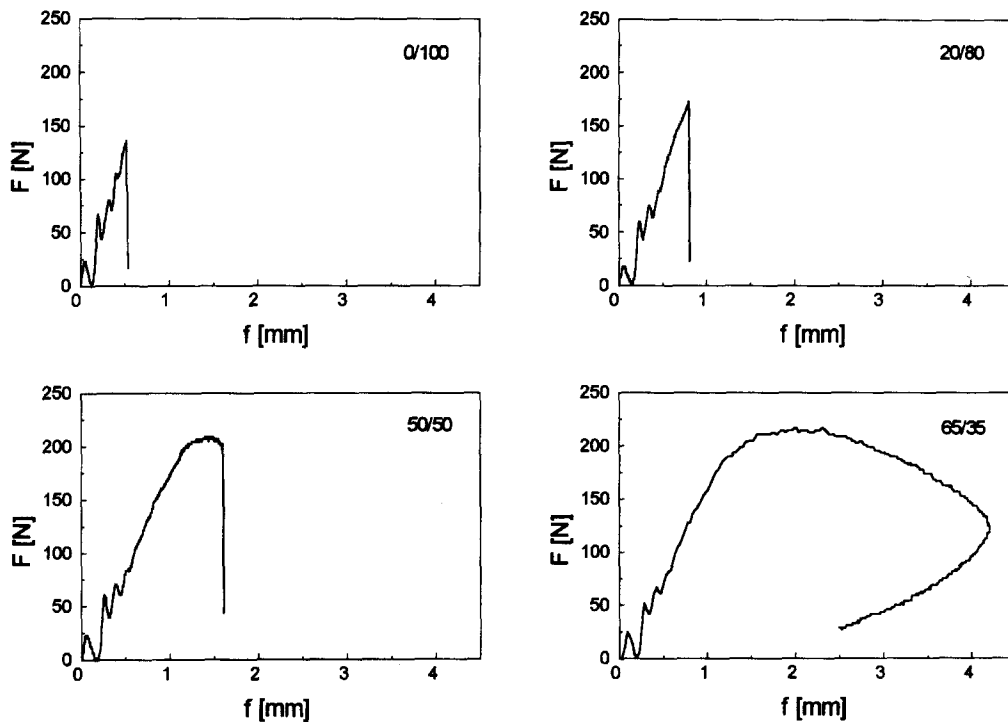


Figure 8 Load (F)-deflection (f)-curves of selected materials recorded during instrumented impact tests at 10°C.

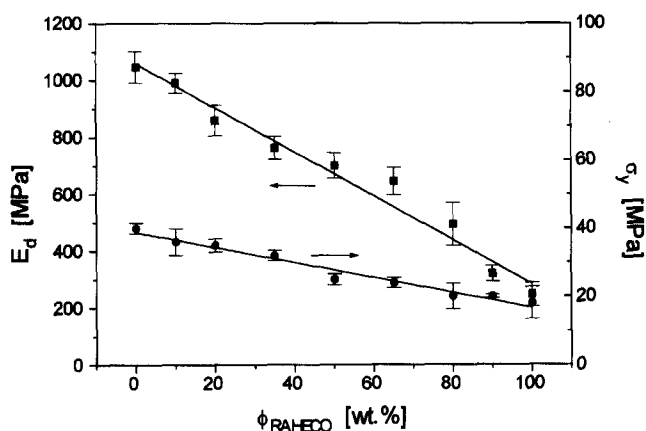


Figure 9 Young's modulus  $E_d$  and dynamic yield stress  $\sigma_y$  versus RAHECO content. The instrumented impact tests were performed at room temperature.

the individual valuation of stable and instable deformation grades, it is possible to avoid an overestimation of material toughness in contrast to the conventional Charpy test<sup>27</sup>. Typical load (F)-deflection (f) curves of materials 65/35, 50/50, 20/80 and 0/100 obtained during instrumented impact tests at 10°C are given in Figure 8.

The diagram shows two transitions of mechanical behaviour. The first transition occurs from pure elastic (material 0/100 and 20/80) to elastic-plastic material behaviour with predominantly instable crack growth (material 50/50). In these regions the specimens break in a brittle manner. The second transition to predominantly stable crack growth without sample fracture is characterised by a strong increase of toughness (for instance, during impact test of material 65/35 at 10°C, Figure 8). The decreasing deflection values at the end of the experiment are caused by reflection of the pendulum striker from the sample. Accordingly, the deformation behaviour changes from brittle to tough, whereas the Young's modulus  $E_d$  and

yield stress  $\sigma_y$ , calculated from load-deflection curves of unnotched specimens, linearly decrease with increasing rubber content (Figure 9). Therefore, the second transition will be designated brittle-to-tough transition.

The strong increase of toughness is also reflected in an intensive increase of J-integral values. In Figure 10, the J-integral values are given as a function of interparticle distance  $A$  over a range of temperature. Figure 10 shows that the brittle-to-tough transition occurs very rapidly at all temperatures. However, there is an obvious shift of transition to smaller interparticle distances with decreasing test temperature. By extrapolation of the curves (Figure 10), critical interparticle distances ( $A_{crit}$ ), at which the increase of toughness begins, can be determined. The values of  $A_{crit}$  which are independent of specimen geometry due to the sample shape and the experimental method applied<sup>23,28</sup>, are represented in Figure 11 versus temperature.

The linear approximation in Figure 11 seems to agree well with the results of Borggreve<sup>10</sup> and Margolina<sup>11</sup>. The critical interparticle distance  $A_{crit}$  increases strongly with temperature and is independent of  $T_g$  of PP. On the basis of experimental data, it is possible to create an empirical equation (4):

$$A_{crit}(T) = 0.8 + 0.023T. \quad (4)$$

In equation (4), differences to the formulation of Margolina<sup>11</sup> exist, since special materials were analysed to create interparticle distance-temperature interrelations. Hence, the constants of equation (4) should be influenced by molecular parameters of the used matrix and rubber material. To specify equation (4), the temperature dependence of brittle-to-tough transitions of several polymer blends based on different materials as well as materials with distinctive morphologies have to be investigated.

The application of the J-integral concept enables an energetic interpretation of the failure behaviour of materials. The calculation of the J-integral includes the analysis of load-determined and deformation-determined parameters.

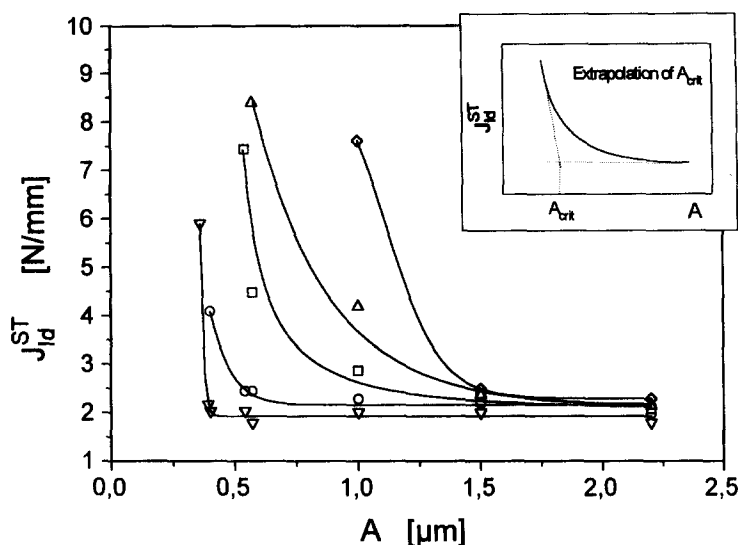


Figure 10 J-integral values  $J_{Id}^{ST}$  versus average interparticle distance  $A$  over a range of temperatures ( $-20^{\circ}\text{C}$  [ $\nabla$ ];  $-10^{\circ}\text{C}$  [ $\circ$ ];  $0^{\circ}\text{C}$  [ $\square$ ];  $10^{\circ}\text{C}$  [ $\triangle$ ];  $23^{\circ}\text{C}$  [ $\diamond$ ]).

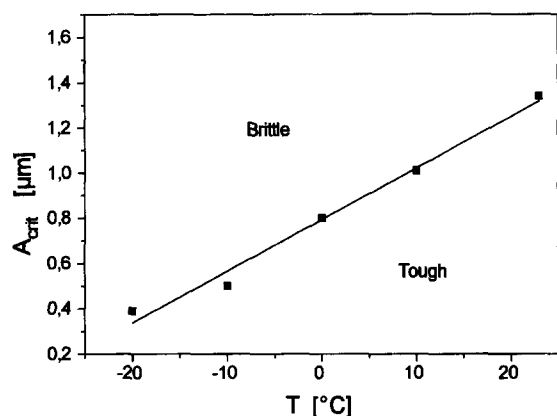


Figure 11 Critical interparticle distance  $A_{crit}$  for brittle-to-tough transition in RAHECO materials versus test temperature  $T$ . The value of  $A_{crit}$  results from extrapolation of curves in Figure 10.

Regarding the linear slope of load-determined  $E_d$  and  $\sigma_y$  values (Figure 9), it can be argued that the observed brittle-to-tough transitions in PP/EPR reactor blends are deformation-induced and consequently dispersion-induced according to the results of Borggreve *et al.*<sup>9</sup>. The phenomenon of brittle-to-tough transition consequently generally follows valid laws. They only differ in quantities, as equation (4) shows. In conclusion, all of the explanations about brittle-to-tough transitions of several polymer blends are qualitatively transferable to heterophasic PP/EPR reactor copolymers. The latter is being considered as a good reference in the PP-based copolymer market.

Comparing the critical interparticle distances of conventional Charpy impact test (CIT) and instrumented Charpy impact test (ICIT) at room temperature, differences are noticeable (CIT:  $A_{crit} \cong 0.8 \mu\text{m}$ ; ICIT:  $A_{crit} \cong 1.3 \mu\text{m}$ ). The disagreement is understandable taking into consideration the experimental differences between both methods. In the case of conventional Charpy tests, the impact strength  $a_{cN}$  considers the deformation energy in an integral manner, whereas the instrumented impact test enables the division of total deformation energy into an elastic and plastic component (*cf.* Equations (1)–(3)) as well as a separate evaluation of fracture toughness as resistance against instable and stable crack growth. Additionally the Charpy

tests were performed at  $2.9 \text{ ms}^{-1}$  impact speed which is nearly two times higher than the pendulum hammer speed of  $1.5 \text{ ms}^{-1}$  during instrumented impact tests. Following that,  $A_{crit}$  shifts to lower values with increasing deformation rate. This tendency corresponds with expectations, however, a quantitative evaluation of the correlation between deformation rate and  $A_{crit}$  has not been realised yet.

#### Micromechanical deformation process

Figures 12 and 13 show HVEM micrographs of *in situ* deformed semi-thin sections of materials 20/80 and 90/10, respectively. The used materials were chosen on the basis of their impact behaviour at room temperature, since the *in situ* tensile tests were performed at the same temperature. Material 20/80 deforms at room temperature in a brittle manner, whereas material 90/10 represents a tough material.

At the beginning of micromechanical *in situ* tests, comparable deformation behaviour can be observed stretching appropriate sections on the HVEM stage. In the unstained sections of this type, the contrast between particles and matrix is obtained from the 'strain induced contrast enhancement' effect. Rubber particles and plastic deformation zones in the matrix are thinner and therefore appear brighter than the elastically deformed matrix material. Cavitation of particles within the EPR layer, situated between the PE inclusions and the PP matrix, was always the first step of deformation. In material 20/80 (Figure 12), the ligaments between the cavitated particles deform by shear yielding processes forming cavitation bands. Note that these cavitation bands are inhomogeneously distributed within the sample. They only arise at isolated positions, whereas the deformation structures in material 90/10 are distributed over the whole sample (Figure 13). In these samples, craze-like structures were created on planes perpendicular to the tensile stress direction, with more extensive fibrillation of the ligaments. The shear flow processes of the matrix polymer are accelerated by the presence of closely-spaced cavitated rubber particles. Structures of this kind, which were observed for the first time in styrene-butadiene block copolymers by Argon *et al.*<sup>29</sup>, have been called 'croids' (from craze and void). So, the transition of impact toughness from brittle to ductile behaviour of bulk materials can be correlated to a transition of micromechanical deformation

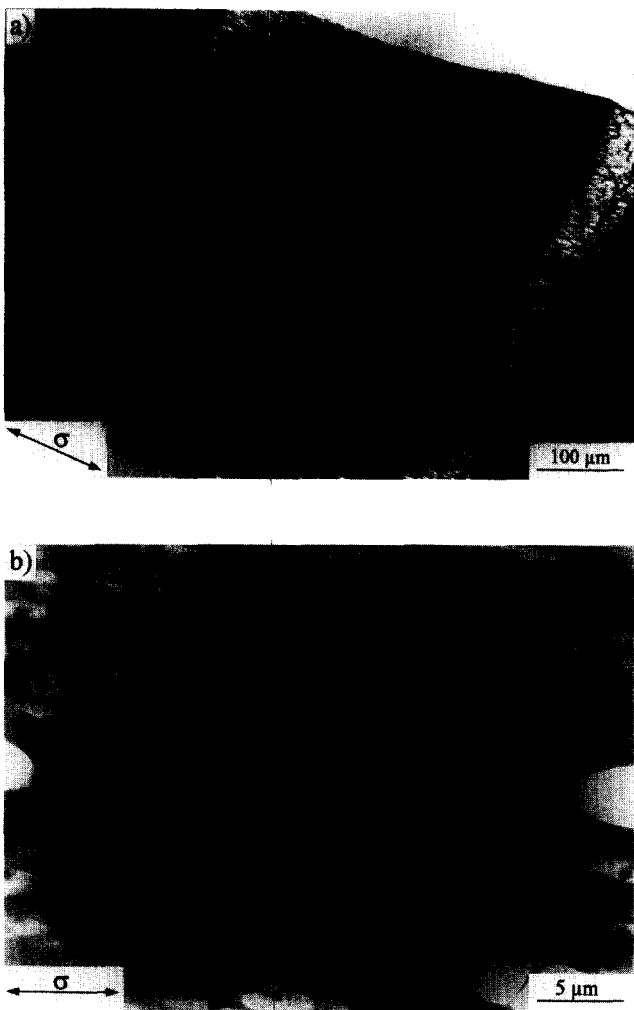


**Figure 12** HVEM micrographs of *in situ* deformed sections of material 20/80. (a) Low magnification-isolated cavitation bands. (b) High magnification-cavitated particles and shear deformation structures between them.

structure in semi-thin sections from cavitation bands to croids.

Furthermore, the results of *in situ* tests suggest that not only the average interparticle distance between cavitated particles but also the distribution of  $A$  should be important to the transition from brittle to tough impact behaviour of the material. Assuming that particles cavitate, if the interparticle distance is smaller than a critical value, the material reacts tougher according to the number of interparticle distances below  $A_{crit}$ . If the number of  $A \leq A_{crit}$  is relatively small, particles cavitate and initiate only isolated deformation structures (croids or cavitation bands). In contrast, the overall deformation of the material is larger if many particles cavitate simultaneously, where they form numerous deformation structures distributed over large sample areas. That means, a homogeneous dispersion of modifier particles with  $A \leq A_{crit}$  will be better than a wide interparticle distance distribution with the same average particle separation.

## CONCLUSIONS

The knowledge of relations between structure and mechanical properties of heterophasic PP/EPR reactor copolymers enables the manufacturer to produce materials with certain

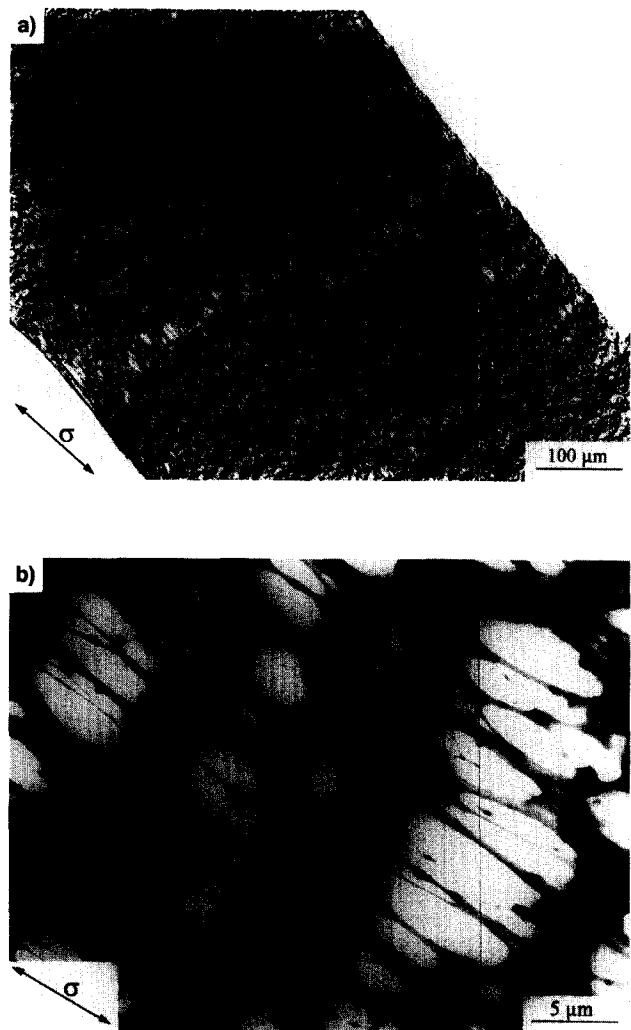


**Figure 13** HVEM micrographs of *in situ* deformed sections of material 90/10. (a) Low magnification-craze-like structures (croids) distributed over the whole sample. (b) High magnification-elongated ligaments between cavitated particles.

morphologies by altering processing conditions. Related to the present results, the structure of the reactor blends could be adjusted, so that the material deforms in a toughened manner at practical operation temperatures.

## ACKNOWLEDGEMENTS

The authors would like to thank the German Research Council (DFG) for financial support of this study which forms part of the research programme 'Innovationskolleg: Grenzschichteigenschaften in Polymerwerkstoffen'. They also thank the 'Max-Planck-Institut fuer Mikrostrukturphysik' in Halle/S. for the opportunity to carry out deformation tests in the 1000 kV high-voltage electron microscope as well as Mr. C. Paulik at PCD Polymere (Linz) for supplying the sample material.

## REFERENCES

1. Ramsteiner, F., *Acta Polymerica*, 1991, **42**, 584.
2. Seiler, E., *Kunststoffe*, 1995, **85**, 1109.
3. Hayashi, K., Morioka, T. and Toki, S., *J. Appl. Polym. Sci.*, 1993, **48**, 411.
4. Neißl, W. and Ledwinka, H., *Kunststoffe*, 1993, **83**, 577.

5. Kim, G. M., Michler, G. H., Gahleitner, M. and Fiebig, J., *J. Appl. Polym. Sci.*, 1996, **60**, 1391.
6. Galli, P., Haylock, J. C. and Simonazzi, T., *Polypropylene: Structure, Blends and Composites*, ed. J. Karger-Kocsis, Chapman and Hall, London, 1995, p. 1.
7. Michler, G. H. and Starke, J. U., *Toughened Plastics II: Science and Engineering*, ed. C. K. Riew and A. J. Kinloch. American Chem. Soc. (ACS Series 252), Washington DC, 1996, Ch. 17, pp. 251–277.
8. Wu, S., *Polymer*, 1985, **26**, 1855.
9. Borggreve, R. J. M., Gaymans, R. J. and Luttmer, A. R., *Makromol Chem., Macromol. Symp.*, 1988, **16**, 195.
10. Borggreve, R. J. M., Gaymans, R. J., Schuijjer, J. and Ingen Housz, J. F., *Polymer*, 1987, **28**, 1489.
11. Margolina, A., *Polym. Commun.*, 1990, **31**, 95.
12. Hopps, S. Y., Bopp, R. C. and Watkins, V. H., *Polym. Eng. Sci.*, 1983, **23**, 381.
13. Sjoerdsma, S. D., *Polym. Commun.*, 1989, **30**, 106.
14. Margolina, A. and Wu, S., *Polymer*, 1988, **29**, 2170.
15. Wu, S. and Margolina, A., *Polymer*, 1990, **31**, 972.
16. Cieslinsky, R. C., *J. Mater. Sci. Letters*, 1992, **11**, 813.
17. Starke, J.U., Godehardt, R., Michler, G.H. and Bucknall, C.B., *J. Mater. Sci.*, 1997, **32**, 1855.
18. Chou, C. J., Vijayan, K., Kirby, D., Hitner, A. and Bear, E. J., *Mater. Sci.*, 1988, **23**, 2533.
19. van der Wal, A. and Gaymans, R. J., *Polymat*, London, 1994, p. 618.
20. Lazzeri, A. and Bucknall, C. B., *Polymer*, 1995, **36**, 2895.
21. Paulik, C., Gahleitner, M. and Neißl, W., *Kunststoffe*, 1996, **86**, 1616.
22. Grellmann, W. and Sommer, J.-P., *Fracture Mechanics and Coupled Fields (FMC-Series)*, Vol. 17, Chemnitz, 1985, p. 48.
23. Grellmann, W. and Seidler, S., *Int. J. Fract.*, 1994, **68**, R19–R22.
24. Merkle, J. G. and Corten, H. T., *ASME J. Pressure Vessel Technol.*, 1974, **6**, 286.
25. Sumpter, J. D. G. and Turner, C. E., *ASTM STP 601*, 1976, p. 3.
26. Grellmann, W., in *Handbuch der Kunststoffprüfung*, ed. H. Schmiedel, Carl Hanser Verlag, München, 1992, p. 139.
27. Grellmann, W. and Che, M., *J. Appl. Polym. Sci.*, in press.
28. Grellmann, W. and Lach, R., *Die angew. Makromol. Chemie.*, 1996, **237**, 191.
29. Argon, A. S., Cohen, R. E., Gebizlioglu, O. S. and Schwier, C. E., in *Advances in Polymer Science 52/53*, ed. H. H. Kausch, Springer Verlag, Heidelberg, 1983, p. 275.